Received: 22 February 2021 | Revised: 19 November 2021 | Accepted: 20 January 2022

DOI: 10.1002/stc.2939

RESEARCH ARTICLE

WILEY

Design and optimization of a novel resonant control law using force feedback for vibration mitigation

Ahmad Paknejad[1] | **Guoying Zhao**[2] | **Simon Chesné**[3] | **Arnaud Deraemaeker**[4] | **Christophe Collette**[1,5]

[1]BEAMS Department, Université Libre de Bruxelles, Brussels, Belgium

[2]MOE Key Laboratory of TianQin Mission, TianQin Research Center for Gravitational Physics & School of Physics and Astronomy, Frontiers Science Center for TianQin, CNSA Research Center for Gravitational Waves, Sun Yat-sen University, Zhuhai, China

[3]LaMCoS, CNRS UMR5259, INSA-Lyon, University of Lyon, Lyon, France

[4]BATir Department, Université Libre de Bruxelles, Brussels, Belgium

[5]Department of Aerospace and Mechanical Engineering, Université de Liège, Liège, Belgium

Correspondence
Ahmad Paknejad, Université Libre de Bruxelles, BEAMS Department, 50 F.D. Roosevelt Av, B-1050 Brussels, Belgium.
Email: ahmad.paknejad@ulb.be

Funding information
Wal'innov, Grant/Award Number: 1610122

Summary

Integral-force-feedback (IFF) is a popular control law in active vibration damping of mechanical system when a force sensor is collocated with a force actuator. While it is simple, robust to resonance uncertainty and stable for any feedback gains, its efficiency is limited by system's parameters and in particular the stiffness ratio between the structure and the actuator. Therefore, the control authority decreases at high frequency resonances or when the actuator is weakly coupled to the structure. It has been shown that the use of double integrator with a real zero, named α-controller, can improve the control authority of a target mode. However, this technique like IFF cannot be easily implemented in practice because of low frequency saturation issue induced by significantly amplifying the low frequency content during the integration process. This paper proposes a new control law, named resonant-force-feedback (RFF), based on a second order low pass filter to damp a target mode resonance. Through the mechanical analogy of the proposed system, RFF can be seen as an active realization of an inerter-spring-damper (ISD) system. In addition, the parameters of RFF are optimized based on two methods, that is, maximum damping criterion and H_∞ optimization which consists in minimizing the settling time of the impulse response and the peak amplitude in the frequency domain, respectively. It is shown that RFF always provides a higher control authority of a target mode in comparison to IFF for a given stiffness ratio and in particular when the stiffness ratio is low. Despite the fact that the performance of the system, in terms of the closed-loop damping ratio or the amplitude reduction, obtained by RFF is very close to that of α-controller, RFF requires less control effort in comparison to α-controller. The stability of the proposed system is also assessed in terms of the gain margin and the phase margin although the system is unconditionally stable. Moreover, the robustness of the designed RFF is compared to that of IFF under stiffness uncertainty. Although IFF can tolerate a higher level of uncertainty, the performance of RFF is superior to that of IFF for almost 50% of changes in the stiffness of the primary system.

KEYWORDS

active control, high performance control, low power consumption control, resonant force feedback, smart structures

1 | INTRODUCTION

Lightweight designs in engineering applications give rise to flexible structures with extremely low internal damping. Vibrations of these flexible structures due to an unwanted excitation of system resonances may lead to high cyclic fatigue failure and noise propagation.[1] A common method to suppress the vibrations is to increase the damping of the system using one of classical control techniques, that is, passive and active.[2] Passive techniques are those control systems which are simply integrated into the structures with no need of additional hardware for their operations, like viscoelastic damping,[3] piezoelectric and electromagnetic shunt damping,[4,5] tuned mass damper[6] etc. However, the control performance of these systems is highly limited to the system properties.[7] For example, viscoelastic damping may not perform well at low frequencies and the performance of shunt damping is dependent on the electromechanical coupling between the structure and the transducer.[8] To overcome the passive limitations, it has been proposed to use active control systems, which are less sensitive to system's parameters, to improve the control performance. It requires an integration of sensors and actuators with a feedback loop containing control laws.[9] The choice of the control law for a system depends on the type of sensor/actuator leading to different shapes of the open-loop transfer function in terms of pole/zero pattern. When an force actuator is combined with a displacement or a velocity sensor as well as when a torque actuator is combined with an angular position or an angular velocity sensor, DVF can be simply used as the control law.[10] For collocated piezoelectric patches used as sensor and actuator, the open-loop transfer function has no high frequency roll-off. Therefore, PPF is often used as the control law to avoid high risk of spill-over at high frequency.[11] For these configurations, the open-loop exhibits alternating poles and zeros, starting with a pole at low frequency. On the other hand, the open-loop transfer function begins with a zero when a force sensor is combined with a force actuator. In this case, it is proposed to apply integral-force-feedback (IFF) as the control law.[12]

It has been shown that IFF is of interest in many engineering applications due to the simplicity of the controller, guaranteed the stability, multimode resonance damping and robustness to resonance uncertainty. Nevertheless, the control performance in terms of maximum achievable damping[12] or maximum amplitude reduction[13] is limited by the distance between the system pole and zero which is a function of the system's stiffness relative to the actuator stiffness. To the best of our knowledge, only a few studies have been focused on the damping improvement of force feedback configurations. Teo and Fleming[14] introduced a feed-through component in the system to increase artificially the distance between the pole and zero and subsequently to improve the maximum modal damping achievable with classical IFF. Chesné et al[15] proposed a new control law (i.e., α-controller) containing double integrator with a real zero to enhance the damping of a target mode. Zhao et al[16] implemented the same control law and used H_∞ criterion to optimize its parameters. Moreover, the potential of using integral force feedback for multiple sensors and actuators has been investigated in Monnier et al[17] based in centralized and decentralized approach.

For a classical active control system, the same or a similar mechanical analogy might be obtained. The mechanical analogy contains passive elements like masses, dashpots, springs, and inerters. Note that inerter is known as a device which generates a force proportional to relative accelerations across its two terminals.[18] This can be used in mechanical designs to modify or substitute the mass of structures. The problem of realizing the mechanical designs passively comes in practical implementations because of some imperfections which will be inevitably present in the mechanical construction preventing them to act as idealized passive elements. For example, springs may have unwanted internal resonances at high frequency[19] which prevents from having high frequency roll-off in the response. Several mechanical forms have been proposed to realize inerters in practice. Two early ideas were to use rack and pinion based inerters[18] as well as ball and screw based inerters.[20] However, their performance may degrade because of the friction and backlash or elastic effect of gears or screws.[21] Hydraulic inerters[22] have been proposed although they may exhibit some nonlinear damping in addition to the inertance-like behavior.[23]

Other than the mechanical analogy of an active control system, it might be possible to obtain an electrical analogy which consists of a piezoelectric or an electromagnetic transducer combined with an electrical network. A well-known example is IFF[24] which is analogous to the relaxation isolator (i.e., its mechanical analogy) as well as an electromagnetic transducer connected to a RL circuit (i.e., its electrical analogy). For piezoelectric transducers, their low capacitance may lead to a large inductance required for the electrical network.[25] The large inductance cannot be easily realized fully passively. Furthermore, high internal resistance of the coil can degrade the performance of the system for electromagnetic transducers.[26]

Realizing the mechanical or the electrical systems by means of active techniques can overcome the aforementioned problems. Tuned inerter damper (TID) system is a well-know mechanical passive control system[27,28] which has been realized semi-actively in Wang et al[29] and actively in Høgsberg et al[30] and Zhao et al.[16] Similar study has been done in Bani-Hani[31] to realize active tuned mass damper (ATMD). In addition, direct acceleration feedback has been introduced in Alujevic et al[32] to synthesize the inerter actively. In Zhao et al,[33] a nonlinear spring has been added to a cantilever beam experimentally by feeding back the displacement of the structure through a cubic function. Moreover, piezoelectric shunt damping has been implemented actively by generating the signal corresponding to the RL circuit digitally.[34] Consequently, active techniques provide us a more flexible tool to shape the behavior of the possible mechanical and electrical systems. Nevertheless, its advantage comes at the expense of a power consumption as an external source is required for actuators.[35]

This paper studies the use of a second order low pass filter as the control law aiming to damp a target mode resonance efficiently. The proposed absorber is named RFF. Optimal parameters of RFF are derived according to the method of maximum damping and H_∞ optimization. These are two classical tuning laws which have been used exclusively for many control problems when their primary systems have no damping. For the method of maximum damping, the parameters are designed such that the closed-loop damping gets maximized accompanied by minimizing the settling time of the impulse response; while for H_∞ optimization, the optimal parameters are set to minimize the maximum steady state response of the structure under harmonic excitation. The optimal parameters are derived in a closed-form formulations for a single-degree-of-freedom (SDOF) system. The efficiency of the optimal formula is evaluated under a multi-degree-of-freedom (MDOF) system. The performance of the designed RFF is evaluated in comparison to that of IFF and α-controller in terms of the control authority, the stability and the robustness to stiffness uncertainties.

The remainder of the paper is organized as follows. In the next section, the mathematical model of the system is derived and then the parameters of the controller are tuned based on the method of maximum damping and H_∞ optimization, separately. The mechanical analogy of the proposed active control system is also introduced in this section as well. Section 3 studies the control effort of the designed system. In Section 4, stability margins of the designed RFF is evaluated and a robustness analysis is studied under stiffness uncertainty. The effeciency of the proposed formula is evaluated under a MDOF in Section 5 The conclusions are drawn in Section 6.

2 | MATHEMATICAL MODELING AND OPTIMIZATION

A typical flexible structure is excited by an external force F_d. An active mount including a force sensor F_s collocated with a piezoelectric stack, and a feedback loop containing the control law $H(s)$ is used for the purpose of vibration damping. Assuming the resonances of the flexible structure are well-separated from each other, the target resonance of the structure can be represented by a SDOF oscillator as shown in Figure 1a. The system is consists of an equivalent mass m and an equivalent stiffness k with no internal damping for the sake of simplicity. It is shown in Figure 1b that the piezoelectric stack can be modeled as a force actuator F_a in parallel to a spring with a stiffness k_a. The governing equations of motion in Laplace domain read:

$$(ms^2 + k)x = F_d + F_s \tag{1a}$$

$$F_s = F_a - k_a x \tag{1b}$$

where s and x are the Laplace variable and the displacement of the mass. Therefore, the transfer function from the actuator to the sensor, when the feedback loop is open, can be derived as follows:

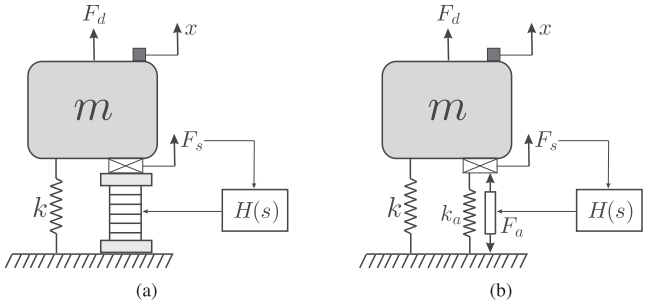

FIGURE 1 (a) Mechanical diagram of the system under consideration including a single-degree-of-freedom (SDOF) system coupled with a force sensor and a piezoelectric actuator. (b) An equivalent model

TABLE 1 Optimal parameters of the system using IFF

Parameters	Maximum damping[12]	H_∞[13]
g_i^{opt}	$\Omega_0\sqrt{\frac{\Omega_0}{\omega_0}}$	$\sqrt{\frac{\Omega_0^2+\omega_0^2}{2}}$
Optimized parameter	$\xi^{opt}=\frac{\Omega_0-\omega_0}{2\Omega_0}$	$\lvert\frac{x}{F_d}\rvert_{max}=\frac{1}{\frac{m}{4}(\Omega_0^2-\omega_0^2)}$

$$G=\frac{F_s}{F_a}=\frac{ms^2+k}{ms^2+k+k_a} \tag{2}$$

which contains a zero at the frequency $\omega_0=\sqrt{\frac{k}{m}}$, representing the resonance frequency of the system when the force sensor is removed, and a pole at the frequency $\Omega_0=\sqrt{\frac{k+k_a}{m}}$, representing the resonance frequency of the coupled system. In addition, the control force F_a is formed like

$$F_a=-H(s)F_s \tag{3}$$

where $H(s)$ is the control law.

2.1 | Integral-force-feedback

A classical control law to damp the resonance of the system is known as IFF which includes an integrator with the gain g_i as follows:

$$H(s)=\frac{g_i}{s} \tag{4}$$

The optimal value of the feedback gain has been already derived analytically based on the maximum damping criterion[12] and H_∞ optimization[13] as shown in Table 1. According to it, it can be concluded that the maximum achievable damping ξ_c^{opt} rapidly decreases and subsequently the minimal maximum of the response $\lvert\frac{x}{F_d}\rvert_{max}$ increases under two conditions. One is for high frequency resonance and the other one is when the actuator is weakly coupled to the structure which leads to a close location of the frequency of the pole Ω_0 and the zero ω_0.

2.2 | α-controller

To improve the control authority, Chesné et al[15] proposed a new control law which includes double integrator and a real zero as shown below:

TABLE 2 Optimal parameters of the system using α-controller

Parameters	Maximum damping[15]	H_∞[16]
g_a^{opt}	$2\sqrt{\Omega_0^2-\omega_0^2}$	$\sqrt{\frac{3(\Omega_0^2-\omega_0^2)}{2}}$
α_a^{opt}	$\frac{\omega_0^2}{2\sqrt{\Omega_0^2-\omega_0^2}}$	$\frac{3\omega_0^2-\Omega_0^2}{\sqrt{6(\Omega_0^2-\omega_0^2)}}$
Optimized parameter	$\xi^{opt}=\frac{\sqrt{\Omega_0^2-\omega_0^2}}{2\omega_0}$	$\lvert\frac{x}{F_d}\rvert_{max}=\sqrt{\frac{2\omega_0^2}{\Omega_0^2-\omega_0^2}}$

$$H(s)=\frac{g_a(s+\alpha_a)}{s^2} \tag{5}$$

where g_a and α_a are its feedback gain and the tuning frequency of its zero. These parameters have been optimized based on the method of maximum damping[15] and H_∞ approach[16] as expressed in Table 2. It can be clearly concluded that for a primary system, α-controller provides a higher closed-loop damping ratio ξ^{opt} and subsequently a lower maximum amplitude of response $|\frac{x}{F_d}|_{max}$ than the classical IFF when the parameters are optimized based on the method of maximum damping and H_∞ approach, respectively. The proposed control system is unconditionally stable as explained in previous works.[12,15]

2.3 | Resonant-force-feedback

In order to avoid a significant amplification of the low frequency content which can be induced by the IFF and the α-controller due to the pure integration, this paper proposes another control law based on a second order filter like:

$$H(s)=\frac{g_f\omega_f^2}{s^2+2\xi_f\omega_f s+\omega_f^2} \tag{6}$$

where g_f is the feedback gain, ξ_f and ω_f are the damping ratio and the tuning frequency of the controller. In this case, the actuator is driven by an active damping force which is generated by making the signal proportional to the force applied to the structure resonate. By substituting Equation (6) into Equation (1), the driving point receptance of the system can be obtained as follows:

$$\frac{x}{F_d}=\frac{s^2+2\xi_f\omega_f s+\omega_f^2+g_f\omega_f^2}{m\Big((s^2+\omega_0)(s^2+2\xi_f\omega_f s+\omega_f^2+g_f\omega_f^2)+(\Omega_0^2-\omega_0^2)(s^2+2\xi_f\omega_f s+\omega_f^2)\Big)} \tag{7}$$

In the reminder of the paper, the following numerical values are used: m=1kg, k=k_a=1N/m, $k_a=0.1k$. In the following sections, mechanical analogies for IFF, α-controller and RFF are first proposed and then two tuning laws based on maximum damping criterion and H_∞ theory are employed to optimize the parameters of RFF. These include the damping ratio ξ_f, the tuning frequency ω_f and the feedback gain g_f.

2.4 | Mechanical analogy

The active mount of the system under consideration is schematically shown in Figure 2a. Considering the Maxwell analogy, force and velocity in the mechanical domain are variables analogous to voltage and current in the electrical

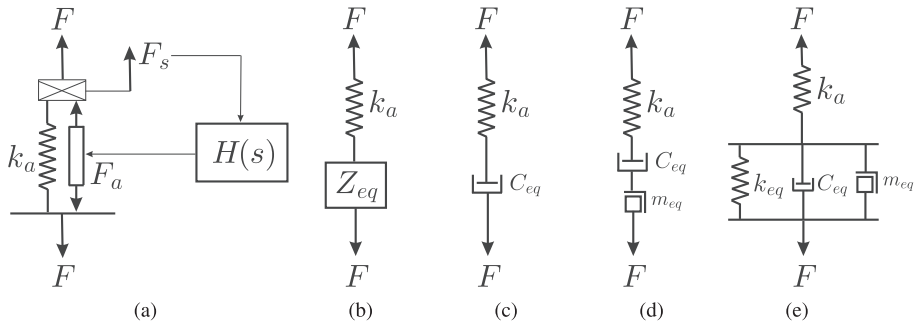

FIGURE 2 (a) Schematic of the active mount. (b) Its equivalent mechanical model. (c) The equivalent mechanical model when integral-force-feedback (IFF) is used. (d) The equivalent mechanical model when α-controller is used.[16] (e) The equivalent mechanical model when resonant-force-feedback (RFF) is used

domain, respectively. Therefore, its total mechanical impedance can be obtained by substituting Equation (3) into Equation (1b) as follows:

$$Z_{T1} = \frac{F}{\dot{x}} = \frac{k_a}{s + s \times H(s)} \tag{8}$$

As presented in Figure 2b, an equivalent mechanical system of the active mount can be exposed as an equivalent impedance Z_{eq} in series to an additional stiffness representing the internal stiffness of the actuator k_a. For such system, the mechanical impedance is given by:

$$Z_{T2} = \frac{F}{\dot{x}} = \frac{k_a}{s + \frac{k_a}{Z_{eq}}} \tag{9}$$

Therefore, the equivalent impedance is obtained by equating Equation (8) and (9) as follows:

$$Z_{eq} = \frac{k_a}{s \times H(s)} \tag{10}$$

The equivalent impedance, when IFF is used, is calculated by substituting Equation (4) into the above equation like:

$$Z_{eq}^{IFF} = \frac{k_a}{g_i} = C_{eq} \tag{11}$$

which presents an equivalent impedance of an viscous damper C_{eq}. As shown in Figure 2c, the mechanical model of the active mount, when IFF is implemented, exhibits the same dynamic system as a relaxation isolator. Thus, the classical IFF can be seen as the active realization of the relaxation isolator. Similar study to realize this dynamic system with an electromagnetic transducer connected to a RL circuit has been introduced in De Marneffe et al.[24] To attain the equivalent impedance of α-controller, Equation (5) is substituted into Equation (10) as follows:

$$Z_{eq}^{\alpha} = \frac{k_a s}{g_a(s + \alpha_a)} = \frac{m_{eq} C_{eq} s}{m_{eq} s + C_{eq}} \tag{12}$$

which represents an equivalent impedance of an inertance m_{eq} in series to a viscous damping C_{eq}. In this case, the mechanical model of the active mount can be considered as tuned-inerter-damper (TID) as shown in Figure 2d. Therefore, α-controller can be seen as the active realization of TID, that is, ATID. ATID has been exclusively discussed in Zhao et al.[16]

For RFF, the equivalent impedance is obtained by substituting Equation (6) into Equation (10) like:

$$Z_{eq}^{RFF} = \frac{k_a}{g_f \omega_f^2} s + \frac{2\xi_f k_a}{g_f \omega_f} + \frac{k_a}{g_f s} = m_{eq} s + C_{eq} + \frac{k_{eq}}{s} \tag{13}$$

which indicates an equivalent impedance of an inertance $m_{eq} = \frac{k_a}{g_f \omega_f^2}$ in parallel to a viscous damping $C_{eq} = \frac{2\xi_f k_a}{g_f \omega_f}$ as well as a stiffness $k_{eq} = \frac{k_a}{g_f}$ as shown in Figure 2e. Clearly, it can be considered as an inerter-spring-damper system known as ISD. Thus, RFF can be seen as active realization of ISD. Note that ISD has been used in vibration isolation,[36] vehicle suspension,[37] railway vehicle suspension,[38] aircraft landing gear suspension.[39] From Equation (13), g_f, ξ_f and ω_f can be obtained as a function of m_{eq}, C_{eq} and k_{eq} as follows:

$$g_f = \frac{k_a}{k_{eq}},\ \xi_f = \frac{C_{eq}}{2\sqrt{m_{eq} k_{eq}}},\ \omega_f = \sqrt{\frac{k_{eq}}{m_{eq}}} \tag{14}$$

where ω_f and ξ_f can be seen as the natural frequency and the damping ratio of ISD, respectively. g_f also shows the stiffness ratio between k_a and k_{eq}. One sees that ISD behaves like a rigid body motion with infinite mass, damping and stiffness when $g \to 0$. Subsequently, it is no longer effective for vibration control and the coupled system resonates at Ω_0. For $g \to \infty$, all the parameters of ISD become zero. Since the stiffness k_a is placed in series to ISD, the whole branch becomes ineffective. Thus, the resulting resonance of the coupled system is the same as the primary system when the active mount is removed, that is, ω_0.

2.5 | Maximum damping optimization of the absorber

In this section, the parameters of the controller are optimized based on the method of maximum damping which consists in minimizing the settling time of the impulse response. Figure 3 shows the root-locus of the loop gain (i.e., $G \times H$) choosing different control parameters. One sees that the controller adds another set of poles to the resulting closed-loop system. Depending on the value of the feedback gain g_f, the closed-loop poles can move individually on two loops starting from the pole of the system as well as the pole of the controller. In addition, the location of the controller pole in the locus is a function of the damping ratio ξ_f and tuning frequency ω_f of the controller which leads to different shape of the loops. By comparing Figure 3c with Figure 3a,b, it can be concluded that the damping of the closed-loop system is locally maximized when the two loops intersect at one point. In this case, the closed-loop poles are merged at the intersection. It is possible to realize an identical closed-loop poles for different target damping by properly tuning the parameters of RFF. This can be seen from Figure 3c,d that the controller which realizes equal closed-loop poles is not unique. However, there is only one controller which makes the loops as large as possible and this occurs when the controller pole is critically damped (i.e., $\xi_f^{opt} = 1$). It should be also noted that the closed-loop system is unconditionally stable for any value of feedback gain, damping ratio and tuning frequency. Similar approach has been used to optimize the parameters of positive-position-feedback (PPF) control system in Paknejad et al.[11] It is worth pointing out that the values of ω_f, ξ_f and g_f are taken arbitrarily to observe the different possible root locus curves in Figure 3. Considering the values of ξ_f and ω_f corresponding to Figure 3c as the local optimum ones, Figure 3a shows a typical root locus of the system when a lower value of ξ_f or ω_f is taken. For a higher value of ξ_f or ω_f, the typical root locus of the system is shown in Figure 3b.

The driving point receptance of the system when the two poles are merged is given by

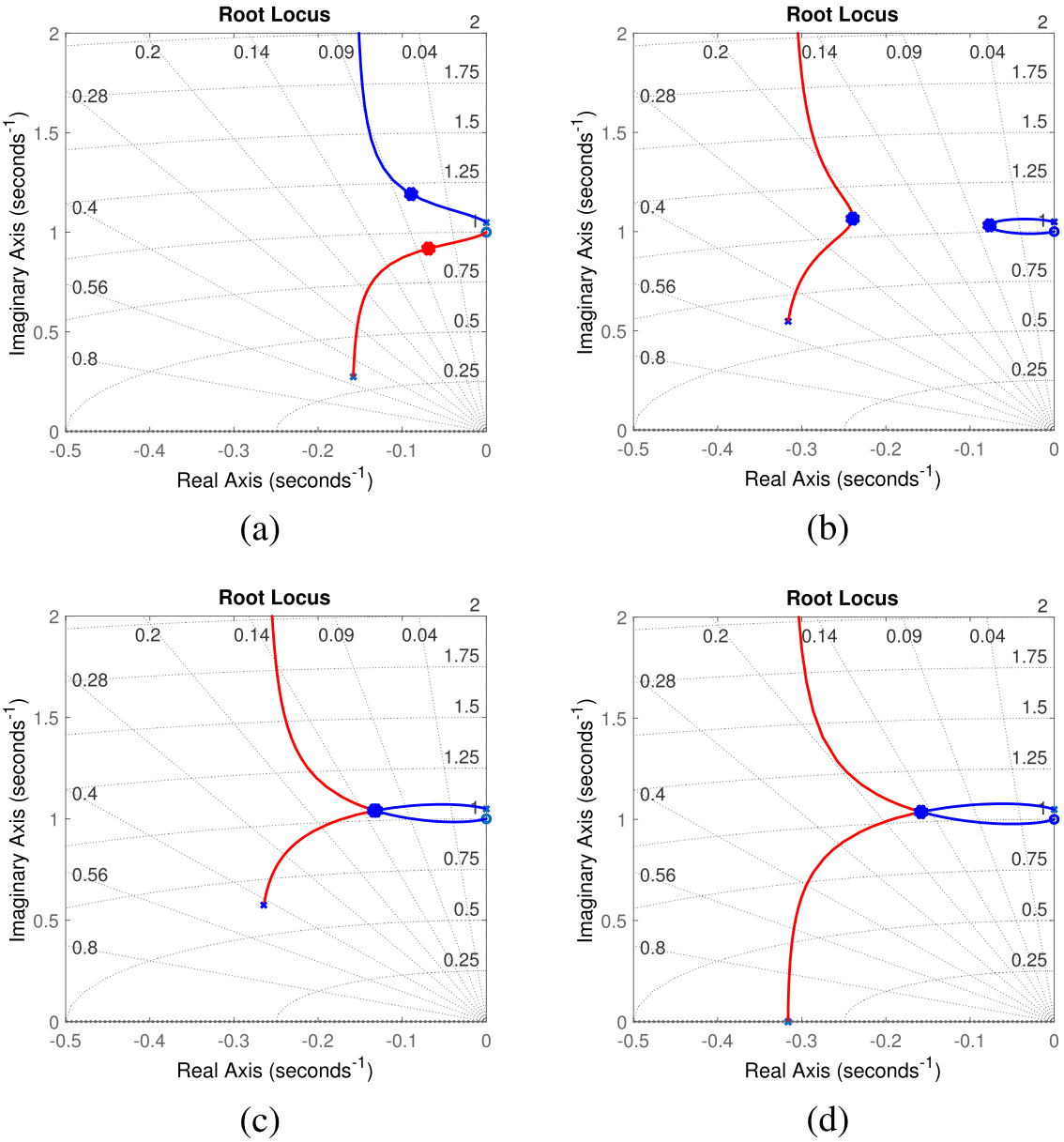

FIGURE 3 Typical root-locus of the system coupled with resonant-force-feedback (RFF) when the tuning frequency and the damping ratio of RFF are set to (a) lower values than those of local optimal case, (b) higher values than those of local optimal case, (c) their local optimal case, (d) their optimal case. (• shows the closed-loop poles)

$$\frac{x}{F_d} = \frac{s^2 + 2\xi_f \omega_f s + \omega^2 + g_f \omega_f^2}{\left(s^2 + 2\xi_c \omega_c s + \omega_c^2\right)^2} \tag{15}$$

where ξ_c and ω_c are the damping ratio and the resonance frequency of the closed-loop system, respectively. The following equations are obtained by equating the characteristic polynomial coefficients of Equations (7) and (15).

$$4\xi_c \omega_c = 2\xi_f \omega_f \tag{16a}$$

$$(4\xi_c^2 + 2)\omega_c^2 = (g_f + 1)\omega_f^2 + \Omega_0^2 \tag{16b}$$

$$4\xi_c\omega_c^3 = 2\xi_f\omega_f\Omega_0^2 \tag{16c}$$

$$\omega_c^4 = g_f\omega_f^2\omega_0^2 + \omega_f^2\Omega_0^2 \tag{16d}$$

Substituting Equation (16a) into Equation (16c) considering $\xi_f = \xi_f^{opt} = 1$ leads to

$$\omega_c = \Omega_0 \tag{17}$$

which means that the resonance frequency of the closed-loop system is the same as the resonance frequency of the system when the feedback loop is open. From Equation (16a), the closed-loop damping ratio can be obtained as a function of tuning frequency of the controller as $\xi_c = \frac{\omega_f}{2\Omega_0}$. Therefore, by substituting it into Equations (16b) and (16d) and solving the resulting equations for the tuning frequency of the controller and the feedback gain, the corresponding optimal parameters of the controller can be derived as follows:

$$\omega_f^{opt} = \sqrt{\Omega_0^2 - \omega_0^2} \tag{18a}$$

$$g_f^{opt} = \frac{\Omega_0^2}{\Omega_0^2 - \omega_0^2} \tag{18b}$$

And subsequently the closed damping ratio can be obtained:

$$\xi_c^{opt} = \frac{\sqrt{\Omega_0^2 - \omega_0^2}}{2\Omega_0} \tag{19}$$

Figure 4 presents the minimum closed-loop damping ratio of the system against the variation of parameters of RFF normalized with respect to their optimal values. Note that when one parameter changes, the other parameters are set to their optimal values. It can be clearly seen that only the optimal parameters provide maximum damping.

As it was already mentioned at the beginning of this section, the goal of the optimization is not only to maximize the closed-loop damping but also to minimize the settling time of the impulse response. Therefore, Figure 5a shows the impulse response of the system for $\xi_f/\xi_f^{opt} : 1/1.3, 1, 1.3$ while the tuning frequency ω_f and the feedback gain g_f are set to their optimal values. Furthermore, the impulse response is demonstrated in Figure 5b for $\omega_f/\omega_f^{opt} : 1/1.3, 1, 1.3$ when ξ and g_f are fixed at their optimal values. In addition, for $g_f/g_f^{opt} : 1/1.3, 1, 1.3$ when ξ_f and ω_f are kept at their optimal

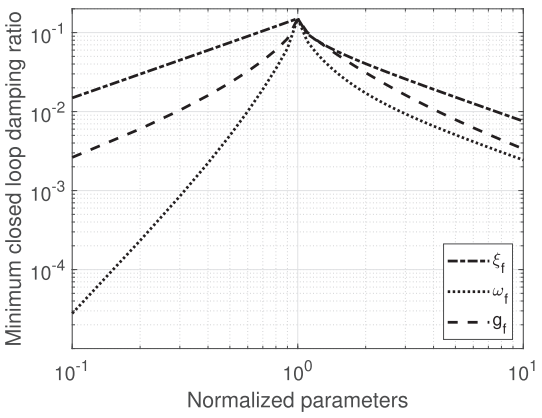

FIGURE 4 Minimum closed-loop damping ratio of the system against the variation of the parameters of resonant-force-feedback (RFF) normalized with respect to their optimal parameters

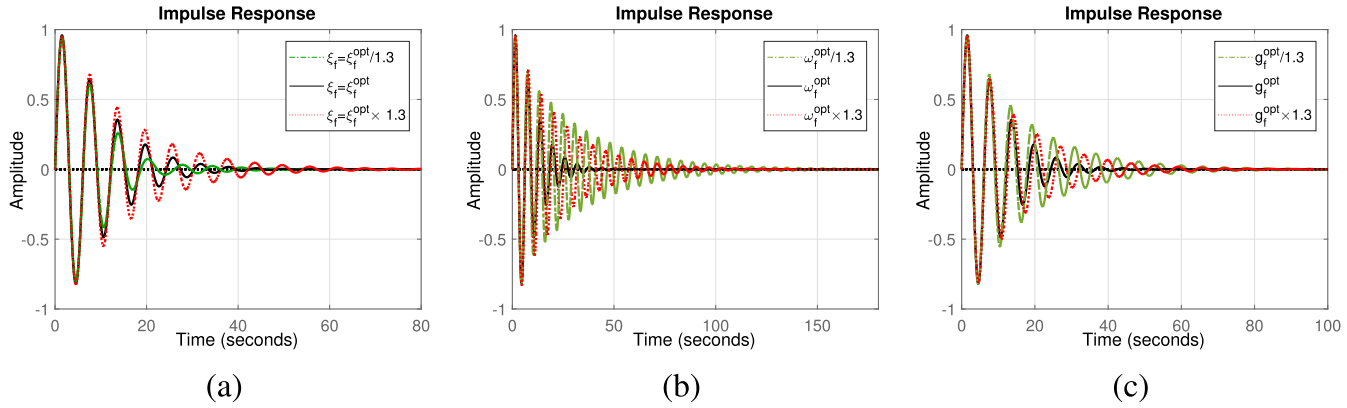

FIGURE 5 Impulse response of the coupled system with resonant-force-feedback (RFF) for different values of (a) damping coefficient ξ_f, (b) tuning frequency ω_f, and (c) feedback gain g_f

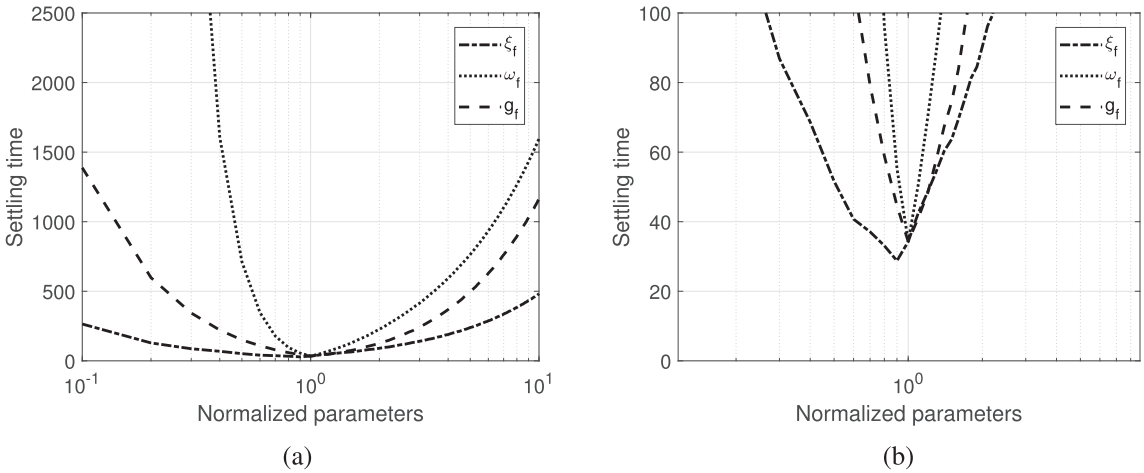

FIGURE 6 (a) Settling time as a function of the variation of the parameters of resonant-force-feedback (RFF) normalized with respect to their optimal values, (b) a zoom from 0 to 100 s

values, Figure 5c illustrates the impulse response. It can be seen that only the optimal values of ω_f and g_f realize the minimum settling time. However, for the case of ξ_f, a lower value offers a better settling time. To better illustrate this issue, the settling time is shown in Figure 6 when the parameters of RFF are varied. 15% reduction in the settling time happens when the damping ratio ξ_f is 10% lower than the optimal value. At this stage, it is not very clear the reason for not having minimum settling time with the maximum damping. Although, this can be related to the fact that the settling time can be dominated not only by the damping ratio but also by the resonance frequency of the system. It gets even more complicated to estimate since the resulting closed-loop system contains two poles with the same damping ratio but different resonance frequencies (according to Figure 3a) when the damping ratio of RFF gets detuned to a lower value. The damping ratio and resonance frequency of both poles can affect the settling time. Therefore, a more careful analysis needs to be done in the future to provide more detail in this subject.

On the other hand, this phenomenon only happens when $\frac{k_a}{k} < 0.5$. For example when $\frac{k_a}{k} = 0.5$, the minimum closed-loop damping ratio and the settling time are plotted against the normalized parameters of RFF in Figure 7a,b, respectively. Obviously, the optimal parameters not only realize the maximum damping but also the minimum settling time. Comparing the performance of the system in terms of the settling time and the minimum closed-loop damping ratio under deviations of the parameters of RFF from the optimal values (Figures 4–7), it can be concluded that the performance of RFF is highly sensitive to the variation of the tuning frequency ω_f. In other words, it shows how robust RFF is under the resonance uncertainty which will be further discussed in Section 4.2.

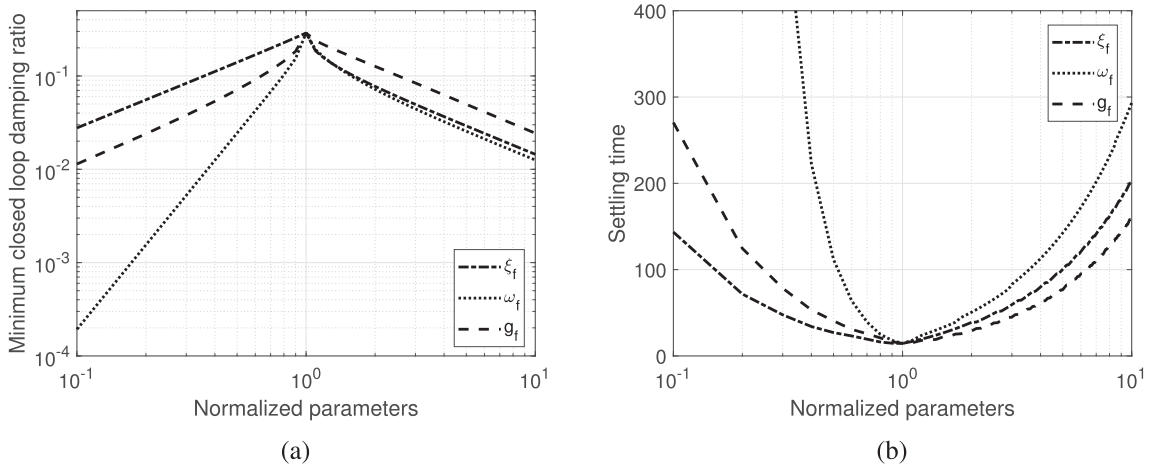

FIGURE 7 Under the variation of the parameters of resonant-force-feedback (RFF) normalized with respect to their optimal parameters when $\frac{k_a}{k} = 0.5$, (a) minimum closed-loop damping ratio and (b) settling time

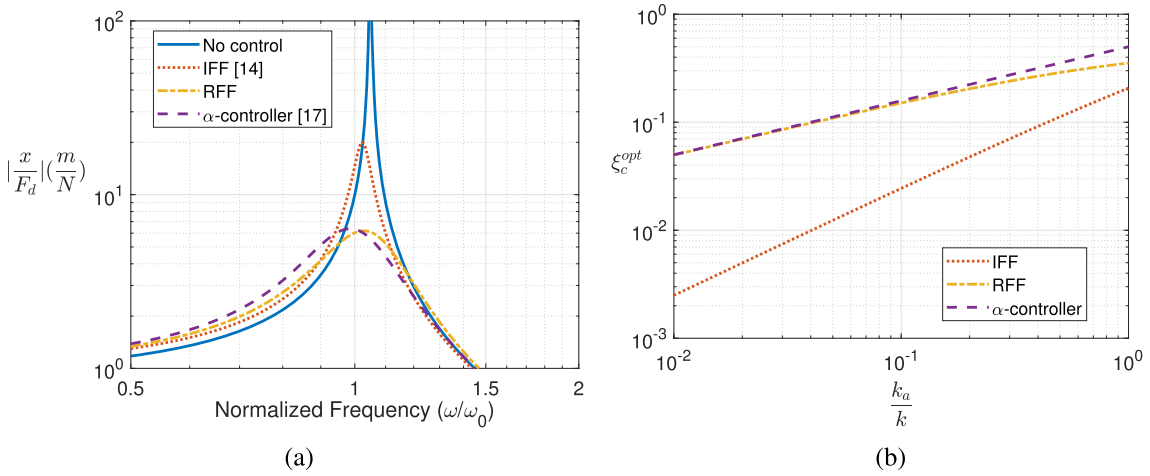

FIGURE 8 When parameters of integral-force-feedback (IFF), α-controller as well as resonant-force-feedback (RFF) are optimized based on the method of maximum damping, (a) frequency-response-function (FRF) of the the performance index with and without control systems for $k_a = 0.1k$, (b) optimal closed-loop damping coefficient ξ_c^{opt} under the variation of the stiffness ratio $\frac{k_a}{k}$

Figure 8a shows the frequency-response-function (FRF) of the performance index with and without control systems. It also compares the performance of RFF with IFF[12] and α-controller[13] when they are optimized based on the method of maximum damping. In order to reveal the difference of using RFF in comparison to IFF and α-controller, Figure 8b presents the evolution of the maximum closed-loop damping ratio under the variation of the stiffness ratio ($\frac{k}{k_a}$). It is explicitly obvious that RFF and α-controller add more damping to the structure in comparison to the one with IFF. The out-performance occurs since both RFF and α-controller introduce an anti-resonance to the primary system allowing a better interaction between the actuator and the primary structure. Considering lightly damped structures where the primary system possess 1% or less damping ratio, it can be concluded that IFF is no longer effective when the stiffness ratio is lower than 5%. However in this case, RFF and α-controller can add at least 10 times greater damping ratio. Another interesting observation is that both RFF and α-controller provide a very close damping ratio especially when the stiffness ratio is low, that is, $\frac{k_a}{k} < 0.2$. This can be seen by the root-locus of the system when α-controller is implemented as shown in Figure 9 for $\frac{k_a}{k} = 0.1$. It shows that the maximum achievable damping ratio, which occurs when the two loops are interesting at one point, is about 15.8%; while RFF can realize 15.1% damping ratio according to Figure 3d. More details on the root-locus of the system coupled with the α-controller under the deviation of its parameters can be found in.[15] Although the α-controller gives a slightly better control authority when $\frac{k_a}{k} > 0.2$, the difference is not major. For example, if $\frac{k_a}{k} = 1$, the closed-loop damping ratios provided by RFF and α-controller are 0.35

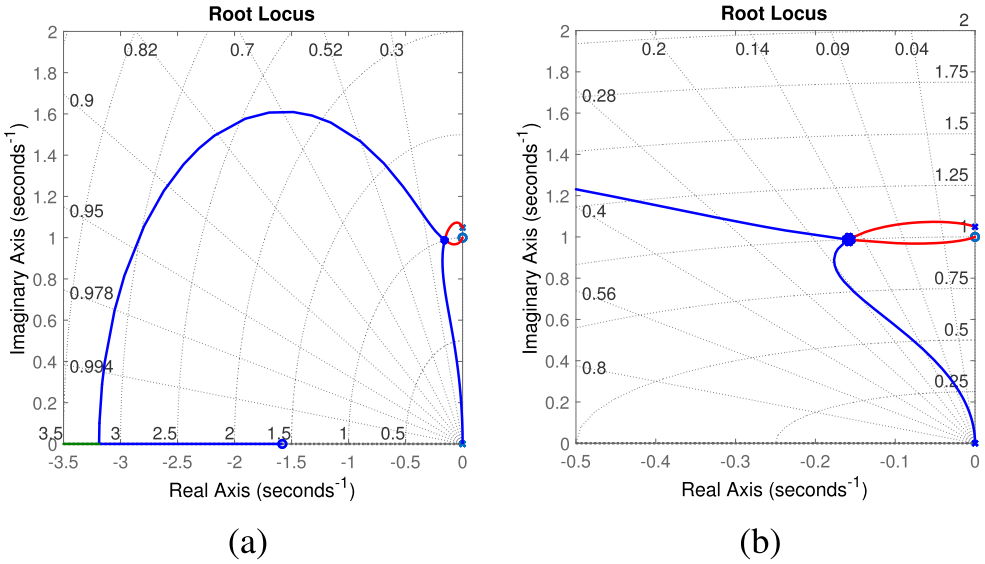

FIGURE 9 (a) Root-locus of the system coupled with α-controller; (b) a zoom on a real axis from -0.5 to 0

and 0.5, respectively. This slightly better damping ratio provided by α-controller affects the stability of the system in terms of phase margin which will be discussed in Section 4.1.

2.6 | H_∞ optimization of the absorber

Another tuning method based on H_∞ optimization is used in this section to optimize the parameters of the controller. The optimization is known as an approximation of fixed-point theory which has been introduced by Den Hartog[40] to optimally design parameters of tuned-mass-damper (TMD) system. The optimization aims to minimize the response at the fixed-points. The fixed-points are defined as those frequencies where the magnitude of the deriving point receptance of the system is invariant with respect to the damping coefficient of the controller ξ_f. The magnitude of the frequency response of the driving point receptance is taken as the performance index and it is given by substituting $s = j\omega$ into Equation (7) as follows:

$$
\begin{aligned}
\left|\frac{x}{F_d}\right| &= \frac{\sqrt{\omega^4 + (4\xi_f^2\omega_f^2 - 2g_f\omega_f^2 - \omega_f^2)\omega^2 + (g_f+1)\omega_f^4}}{m\sqrt{D_8\omega^8 + D_7\omega^7 + D_6\omega^6 + D_5\omega^5 + D_4\omega^4 + D_3\omega^3 + D_2\omega^2 + D_1\omega + D_0}} \\
D_8 &= 1; D_7 = D_5 = D_3 = D_1 = 0 \\
D_6 &= 2(2\xi_f^4 - g_f - 1)\omega_f^2 - 2\Omega_0^2 \\
D_4 &= (g_f+1)^2\omega_f^4 - (8\xi_f^2\Omega_0^2 - 2g_f(\Omega_0^2+\omega_0^2) - 4\Omega_0^2)\omega_f^2 + \Omega_0^4 \\
D_2 &= (4\xi_f^2\Omega_0^4 - 2g_f\omega_0^2\Omega_0^2 - 2\Omega_0^4)\omega_f^2 - (2g_f^2\omega_0^2 + 2g_f(\Omega_0^2+\omega_0^2) + 2\Omega_0^2)\omega_f^4 \\
D_0 &= (g_f\omega_0^2 + \Omega_0^2)^2\omega_f^4
\end{aligned}
\tag{20a}
$$

The fixed-point frequencies are obtained by differentiating the above equation with respect to the damping coefficient ξ_f and equating the derivative to zero, which yields:

$$
\Omega_1 = \frac{1}{\sqrt{2}}\sqrt{(g_f+1)\omega_f^2 + \Omega_0^2 - \sqrt{(g_f+1)^2\omega_f^4 - 2g_f\omega_0^2\omega_f^2 - 2\Omega_0^2\omega_f^2 + \Omega_0^4}} \tag{21a}
$$

$$\Omega_2 = \frac{1}{\sqrt{2}}\sqrt{(g_f+1)\omega_f^2 + \Omega_0^2 + \sqrt{(g_f+1)^2\omega_f^4 - 2g_f\omega_0^2\omega_f^2 - 2\Omega_0^2\omega_f^2 + \Omega_0^4}} \tag{21b}$$

$$\Omega_3 = 0 \tag{21c}$$

The third fixed-point Ω_3 is neglected in the following process as it is basically invariant with respect to the parameters of RFF. The optimal value of the tuning frequency ω_f is defined as the one which realizes equal performance at the fixed-point frequencies. This can be obtained by substituting Equations (21)a and (21)b into Equation (20) and equating the resulting expressions for a $\xi_f = 0$, which yields:

$$\omega_f^{opt} = \frac{\Omega_0}{\sqrt{g_f+1}} \tag{22}$$

The performance index at fixed-points does not change for any value of the damping coefficient through the whole frequency range. Therefore, the optimal value of the damping ratio ξ_f is obtained by passing the performance index horizontally through the fixed-points. Two optimal damping coefficients corresponding to two fixed-points can be obtained as follows:

$$\xi_{f1} = \frac{\sqrt{H_1 g_f\left(H_2(g_f+1) - H_1 g_f + 2\sqrt{H_1 g_f\left(-2H_2(g_f+1) + (2(g_f+1))\Omega_0^2 + H_1 g_f\right)}\right)}}{2\sqrt{2H_2(g_f+1)\Omega_0^2 + H_1 H_2 g_f - 4H_1 g_f \Omega_0^2}} \tag{23a}$$

$$\xi_{f2} = \frac{\sqrt{H_1 g_f\left(H_2(g_f+1) + H_1 g_f + 2\sqrt{H_1 g_f\left(2H_2(g_f+1) + (2(g_f+1))\Omega_0^2 + H_1 g_f\right)}\right)}}{2\sqrt{2H_2(g_f+1)\Omega_0^2 + H_1 H_2 g_f + 4H_1 g_f \Omega_0^2}} \tag{23b}$$

$$H_1 = \Omega_0^2 - \omega_0^2$$
$$H_2 = \Omega_2^2 - \Omega_1^2$$

In practice, the optimal value of the damping is considered by taking the quadratic average of the two obtained damping ratio Equations (23)a and (23)b:

$$\xi_f^{opt} = \sqrt{\frac{\xi_{f2}^2 + \xi_{f1}^2}{2}} \tag{24}$$

The optimal value of the feedback gain g_f still needs to be obtained. Figure 10a illustrates the maximum amplitude of the response against the feedback gain g_f when the tuning frequency ω_f and the damping ratio ξ_f are set to their optimal values. It can be clearly seen that the maximum amplitude of response starts to decrease by increasing g_f. However, it stops decreasing after a certain value of a feedback gain which can be introduced as its optimal value. Figure 10b shows the frequency-response-function (FRF) of the performance index for five different values of the feedback gain g_f : 0.1, 1, 28.0459, 30, ∞ when the other two parameters (ω_f and ξ_f) follow their optimal values. One sees that the optimal parameters of the damping ratio ξ_f^{opt} and tuning frequency ω_f^{opt} can realize equal peak for each value of the feedback gain g_f. In addition, the performance index indeed decreases with an increase in the feedback gain until the damping ratio reaches the critical damping. By increasing the feedback gain more, the resonance of the system is shifted slightly to a lower value with a negligible change in the amplitude of response. Therefore, the minimum feedback gain g_f, which realizes the minimal maximum amplitude of response, is defined as the optimal feedback gain. This

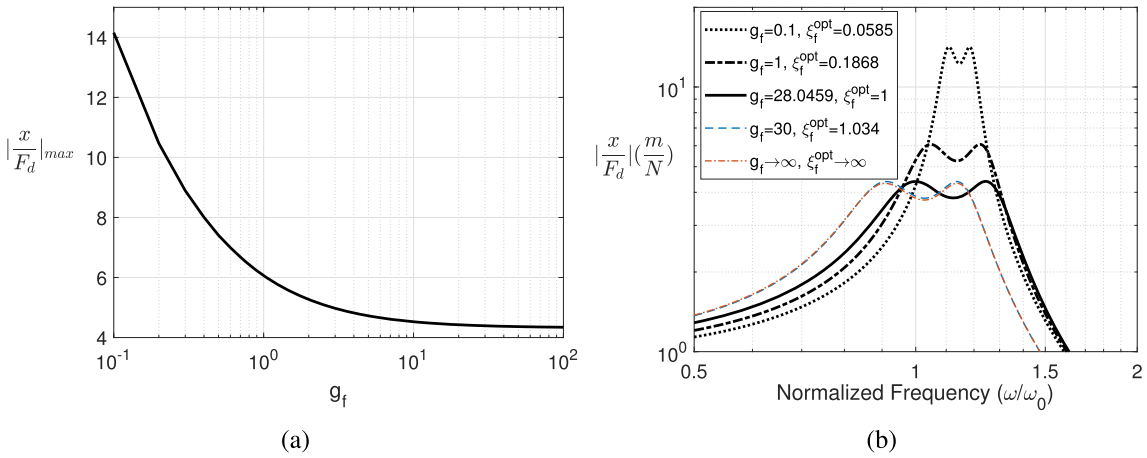

FIGURE 10 (a) Maximum amplitude of response against the feedback gain g_f. (b) frequency-response-function (FRF) of the performance index for different values of the feedback gain g_f when the other parameters follow their optimal values

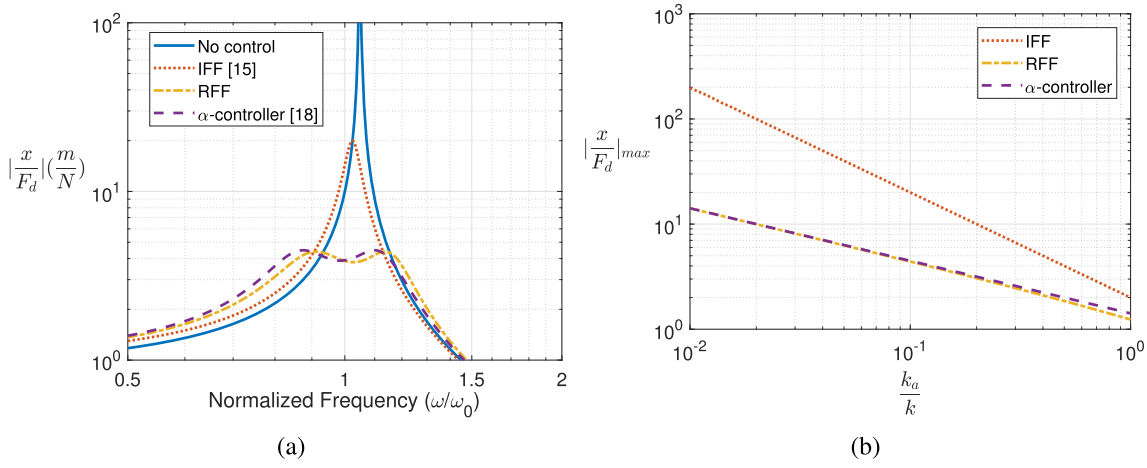

FIGURE 11 When parameters of integral-force-feedback (IFF), α-controller as well as resonant-force-feedback (RFF) are tuned based on H_∞ optimization, (a) frequency-response-function (FRF) of the performance index with and without control systems for $k_a = 0.1k$, (b) maximum amplitude of the performance index under the variation of the stiffness ratio $\frac{k_a}{k}$

occurs when the damping coefficients reaches the critical value. By equalizing Equation (24) to one and solving the resulting equation, the optimal value of the feedback gain is given by:

$$g_f^{opt} = \frac{\Omega_0^2 + 7\omega_0^2 + \sqrt{64\omega_0^4 + 112\omega_0^2(\Omega_0^2 - \omega_0^2) + 97(\Omega_0^2 - \omega_0^2)^2)}}{6(\Omega_0^2 - \omega_0^2)} \tag{25}$$

Figure 11a illustrates FRF of the performance index with and without control systems to compare the vibration attenuation brought by IFF, α-controller and RFF when they are tuned based on H_∞ optimization. It can be seen that the maximum amplitude of the response associated with RFF or α-controller is more than four times lower than the one with IFF. This plot is also interesting because it demonstrates that both α-controller and RFF realize equal peak with slightly different frequencies. To better understand the difference between the performance of the control laws, Figure 11b presents the maximum amplitude of the performance index as a function of the stiffness ratio when parameters are tuned based on H_∞ optimization. It is clearly visible that RFF and α-controller always offer a better amplitude

reduction especially when the coupling between the actuator and the structure is low (i.e. $\frac{k}{k_a} < 0.1$). For example, RFF or α-controller is able to reduce the amplitude of response 10 times lower than the one with IFF when the stiffness ratio is about 2%. An additional observation from this plot is that the vibration attenuation brought by RFF and α-controller is very close to each other especially for $\frac{k_a}{k} < 0.5$. For high stiffness ratio, the difference gets slightly larger such that when $\frac{k_a}{k} = 1$, the maximum amplitude of response is 1.23 and 1.41 with the application of RFF and α-controller, respectively.

It is worth pointing out that the application of RFF results in a dynamically softer system because of a higher static response with respect to that of control-off. This can be justified using the mechanical analogy of RFF shown in Figure 2e. At low frequency, RFF behaves like two stiffness (i.e. k_a and k_{eq}) which are placed in series with each other. In this case, the stiffness of the branch is equal to $\frac{k_a}{1+g_f}$ which is lower than k_a.

It is also interesting to see how sensitive the performance of the system is when RFF is detuned. Figure 12a shows the FRF for five different damping ratios as $\xi_f/\xi_f^{opt}: 0, 0.25, 1, 4, \infty$, while the other parameters are set to their optimal values. The fixed-points can be seen at two frequencies where all the curves are interesting. For $\xi_f < \xi_f^{opt}$, two resonances with higher peaks appear in the vicinity of the primary one; whereas, only one resonance peak can be seen when $\xi_f > \xi_f^{opt}$. It is aligned with the RFF's mechanical analogy shown in Figure 2e. According to Equation (14) when $\xi_f \to 0$, the equivalent damping approaches the zero value ($\equiv C_{eq} \to 0$) while the equivalent inertance and the stiffness are non-zero value ($\equiv m_{eq} \neq 0$ and $k_{eq} \neq 0$). This means that RFF adds another undamped DOF to the system. However, $C_{eq} \to \infty$ when $\xi_f \to \infty$ as well. Therefore, RFF is no longer effective and the system resonates at the resonance frequency of the primary system ($\equiv \Omega_0$). The performance degradation of RFF under the variation of the tuning frequency ω_f is demonstrated in Figure 12b for five different values as: $\omega_f/\omega_f^{opt}: 0, 0.75, 1, 1.33, \infty$, when ξ_f and g_f are set to their optimal values. Moreover, to see how the performance is degraded when the feedback gain is detuned, the FRF is plotted for five different values as: $g_f/g_f^{opt}: 0, 0.5, 2, \infty$ accompanied by fixing the other parameters to their optimal values. RFF gets detuned in the same way by the variation of the tuning frequency or the feedback gain such that the one peak increases accompanied by decreasing the other one. When $\omega_f \to 0$, it is equivalent to infinite value of the inertance and the damping ($\equiv m_{eq}, C_{eq} \to \infty$). Furthermore, when $g_f \to 0$, all the equivalent parameters go to infinite value ($\equiv m_{eq}, C_{eq}, k_{eq} \to \infty$). In both cases, similar to $\xi_f \to \infty$, RFF is no longer effective and the system keeps resonating at the resonance frequency of the primary system ($\equiv \Omega_0$). On the other hand when $\omega_f \to \infty$, RFF degrades to a non-zero value stiffness ($\equiv k_{eq} \neq 0$) causing a reduction in the resonance frequency since the equivalent stiffness is placed in series to the stiffness of the actuator. The total stiffness of the branch (Figure 2e) is now equal to $\frac{k_a}{1+g_f}$. In the case of $g_f \to \infty$, the impedance of RFF becomes zero such that no force will pass through the branch (Figure 2e) as if it is removed from the system. Hence, the resonance frequency of the system is equal to the resonance frequency of the primary system when the force sensor is taken away ($\equiv \omega_0$). It is worth pointing out that the amplitude of response is more sensitive to the tuning frequency than the others because the peaks get detuned rapidly by slightly deviating from its optimum.

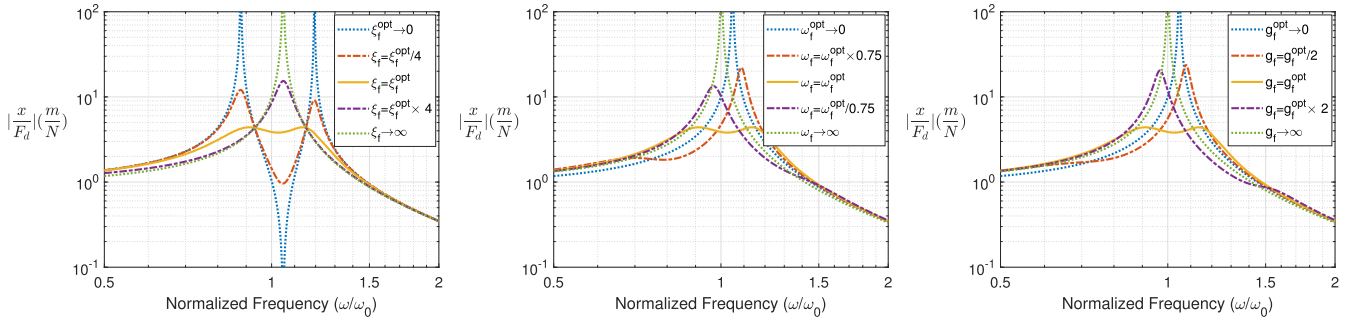

FIGURE 12 Frequency-response-function (FRF) of the performance index for different values of (a) the damping ratio ξ_f, (b) tuning frequency ω_f and (c) feedback gain g_f when the other parameters are set to their optimal values

3 | CONTROL EFFORT

It has been shown in the previous section that both RFF and α-controller provide almost the same control authority to the system. The difference between them can be expressed in the terms of the control effort. To do so, the actuator force with respect to the input disturbance force is taken as the performance function. This performance function can be obtained using Equations (1) and (3) as follows:

$$\frac{F_a}{F_d} = \frac{k_a H(s)}{(ms^2+k)(1+H(s))+1} \tag{26}$$

By substituting Equations (5) and (6) into the above equation,respectively, the performance function for α-controller and RFF can be obtained as follow:

$$\frac{F_a}{F_d} = \frac{k_a g_a(s+\alpha)}{(ms^2+k)(s^2+g_a(s+\alpha))+s^2} \tag{27a}$$

$$\frac{F_a}{F_d} = \frac{k_a g_f \omega_f^2}{(ms^2+k)(s^2+2\xi_f\omega_f s+\omega_f^2+g_f\omega_f^2)+s^2+2\xi_f\omega_f s+\omega_f^2} \tag{27b}$$

Figure 13a,b shows the FRF of the actuator force when parameters are optimized according to the method of maximum damping and H_∞ approach, respectively. It can be clearly seen that α-controller requires a higher actuator force than that of RFF. In addition, the maximum actuator force corresponding to α-controller is 2.67 and 2.54 greater than that of RFF when the parameters are tuned according to the method maximum damping and H_∞ approach, respectively. In other words, the amount of current needs to be delivered to the actuator for α-controller is higher than that of RFF and subsequently it consumes more power.

According to Figure 13a,b, no matter which optimization criterion is used, two peaks appear in the magnitude of the force around the resonance frequency of the system for both RFF and α-controller. At the first peak, RFF requires less force than α-controller while it is the other way around at the second peak. In addition, the magnitude of actuator force contains a non-zero constant value at low frequency. It is worthwhile noting that this low frequency force interacts on the stiffness of the structure leading to a dynamically softer system as it has been already observed in the previous section from Figures 8a and 11a where the static response has increased. For both optimization criteria, α-controller requires a higher actuator force than that of RFF at low frequency. Therefore, other than the power needs to be given to the actuator for reducing the resonance peak, an amount of current needs to be provided for the actuator for the low frequency force. Since α-controller requires more force at low frequency than RFF, low frequency force has

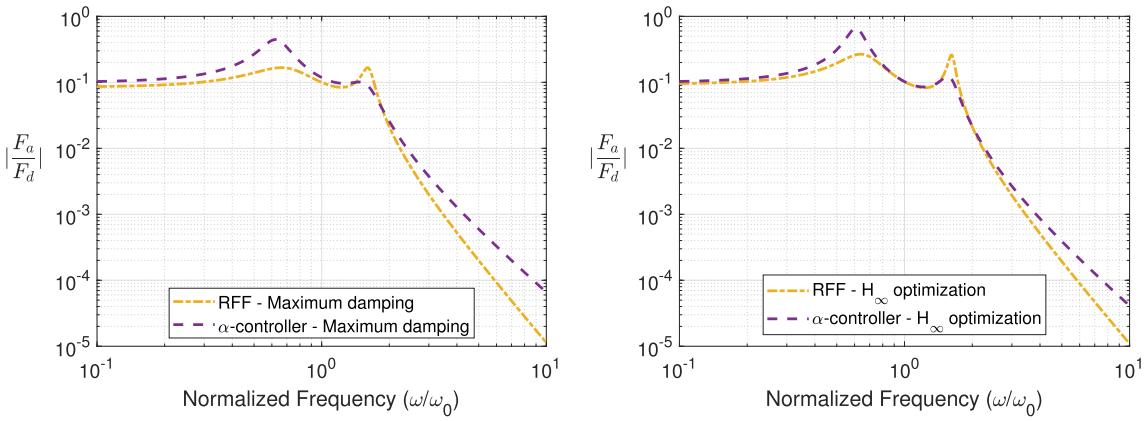

FIGURE 13 FRF of the actuator force, (a) when the parameters are optimized according to the method of maximum damping, (b) when the parameters are tuned based on H_∞ optimization

a big impact on the total power consumption of the control system. Even at high frequency, the control force corresponding to α-controller is higher than that of RFF, although it can be neglected because of more than three order of magnitude difference compared to the low frequency force. It is clear that a criterion, which is able to consider the actuator force over the frequency-band of interest ($\pm\infty$), is required to compare RFF with α-controller. H_2 norm measures the energy of the actuator force through the whole frequency range. Consequently, H_2 norm is proposed for further comparison and it is assessed as follows:[41]

$$||F_a||_2 = \sqrt{\frac{1}{2\pi}\int_{-\infty}^{\infty} F_d(\omega)\left|\frac{k_a H(j\omega)}{(-m\omega^2+k)(1+H(j\omega))+1}\right|^2 d\omega} \tag{28}$$

where $F_d(\omega)$ is the power spectral density of the input disturbance force. For the case of white noise excitation force, it is constant as a function of the frequency, that is, $f_d(\omega) = f_d$. Therefore, the H_2 norm can be simplified as follows:

$$||F_a||_2 = \sqrt{\frac{F_d}{2\pi}\int_{-\infty}^{\infty}\left|\frac{k_a H(j\omega)}{(-m\omega^2+k)(1+H(j\omega))+1}\right|^2 d\omega} \tag{29}$$

In other words, the above equation represents the root-mean-square (RMS) value of the actuator force. Then, its normalized I_{nor} is defined to highlight the ratio of the RMS of the actuator force to the excitation force with a uniform spectral density like:

$$I_{nor} = \sqrt{\frac{\pi}{F_d}}||F_a||_2 = \sqrt{\int_0^{\infty}\left|\frac{k_a H(j\omega)}{(-m\omega^2+k)(1+H(j\omega))+1}\right|^2 d\omega} \tag{30}$$

Figure 14a,b present I_{nor} under the variation of the stiffness ratio when parameters are optimized according to the method of maximum damping and H_∞ approach, respectively. Two observations can be made on this plot. One sees that α-controller always requires a higher actuator force than RFF especially when the stiffness ratio increases. In addition, the actuator force of RFF when its parameters are tuned based on H_∞ optimization is greater than that of RFF when its parameters are optimized based on the method of maximum damping. However, this is not the case for α-controller. For a vary low stiffness ratio $\frac{k_a}{k} << 0.1$, it slightly requires less actuator force when its parameters are optimized based on the method of maximum damping. It is the opposite for high value of the stiffness ratio $\frac{k_a}{k} \gg 0.1$.

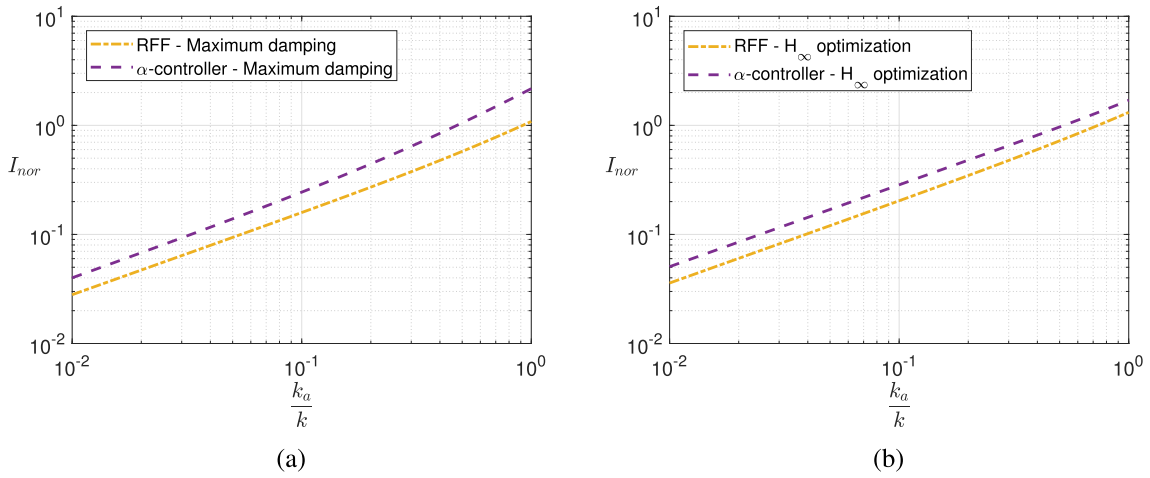

FIGURE 14 Normalized root mean square value of the actuator force I_{nor} versus the variation of the stiffness ratio $\frac{k_a}{k}$ (a) when the parameters are optimized according to the method of maximum damping and (b) when the parameters are tuned based on H_∞ optimization

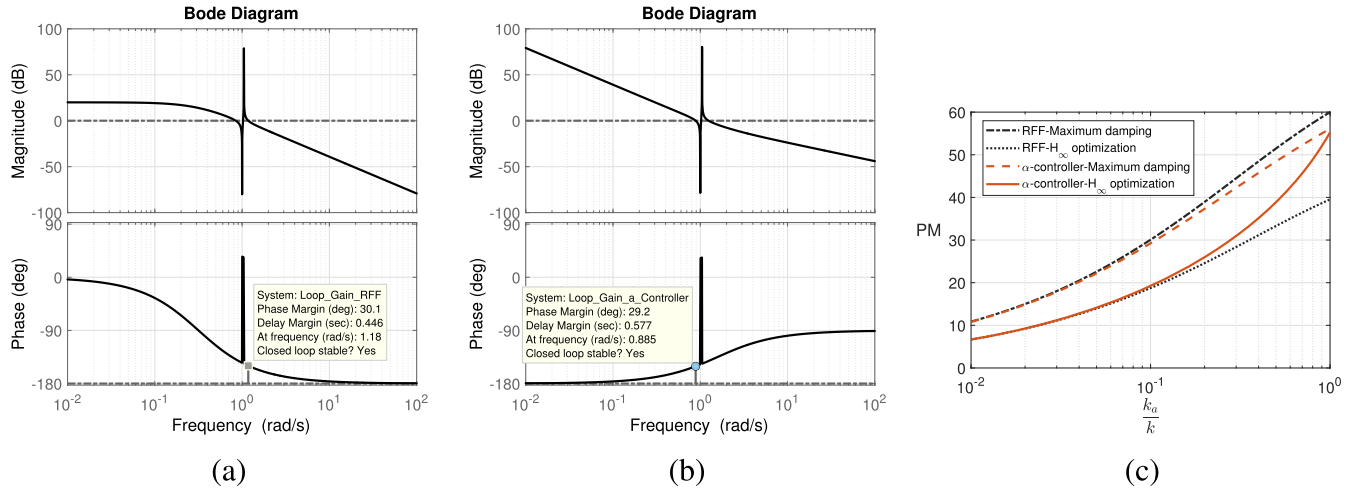

FIGURE 15 The bode diagram of the loop-gain ($G \times H$) when the parameters of resonant-force-feedback (RFF) are tuned according to the method of the maximum damping and when the parameters of α-controller are tuned according to. (c) Minimum phase margin with respect to the stiffness ratio when the parameters are set to their optimal values

4 | STABILITY AND ROBUSTNESS ANALYSIS

4.1 | Stability analysis

It is always important to estimate the gain margin and the phase margin of a control system even if it is unconditionally stable like RFF. Enough margins could avoid an instability of the system in practical implementation. The bode diagram of the loop-gain (i.e., $G \times H$) is shown in Figure 15a when RFF is tuned according to the method of maximum damping. The minimum stability margin is also highlighted in the figure. Clearly, the gain margin is infinity and the phase margin is 30.1°. Similarly, for H_∞ optimization, the phase margin is 18.7°. Furthermore, the loop-gain of the system when α-controller is implemented is shown in Figure 15b when the parameters are optimized based on the maximum damping. Like RFF, the gain margin is infinity. However, the minimum phase margin is 29.2°. Similarly, for the H_∞ methods, the phase margin is 19.2°. Furthermore, α-controller significantly amplifies the low frequency content due to the use of pure integration while this is not the case for RFF. This amplification of response can easily cause the saturation of the actuator in the practical implementation of α-controller.

Those bode diagrams are obtained for a certain value of the stiffness ratio, that is, $\frac{k_a}{k} = 0.1$. The evolution of the minimum phase margin when the stiffness ratio $\frac{k_a}{k}$ is varied and the parameters of RFF and α-controller follow their optimal values is demonstrated in Figure 15c. According to it, three important observations are made. First, the method of maximum damping always offers a better phase margin than that of H_∞ approach. Furthermore, the minimum phase margin decreases by reducing the stiffness ratio. Noted that the classical IFF maintains an infinite gain margin and 90° phase margin for any value of the feedback gain. It can be concluded that the better control performance obtained by RFF or α-controller than IFF, as explained in Section 2, comes at the expense of a degradation in the phase margin. Moreover, Figure 15c is connected to Figures 8b and 11b. In Figure 8b, it has been shown that α-controller gives a slightly better control performance in terms of the closed-loop damping ratio than RFF for high value of the stiffness ratio. This out-performance is reflected directly in the minimum phase margin shown in Figure 15c. It is the other way around when the parameters are tuned according to H_∞ optimization. According to Figures 11b and 15c, the better control performance provided by RFF in terms of the amplitude reduction comes at the price of a lower phase margin compared to that of α-controller.

4.2 | Robustness analysis

What follows is a robustness study of IFF, α-controller, and RFF under the stiffness uncertainty. To check the robustness of the systems based on the method of maximum damping, the minimum damping ratio of the closed-loop system,

named μ, is shown in Figure 16a under the variation of the stiffness of the primary system k normalized with respect to the initial value $k = k_0 = 1$. In addition, the normalized maximum amplitude of the response with respect to its static response (i.e., $Y = (k + k_a)|\frac{x}{F_d}|_{max}$) is considered for the robustness analysis of the systems designed based on H_∞ optimization. Figure 16b shows Y against $\frac{k}{k_0}$. In both figures, the robustness is evaluated for three different stiffness ratio $k_a/k_0 : 0.01, 0.1, 1$ while the corresponding optimal parameters of RFF, α-controller, and IFF are tuned for $k = k_0$ and kept constant. For $k < k_0$, it is interesting that the closed-loop damping μ realized by IFF started to increase and subsequently the maximum amplitude of response at the frequency of resonance decreases with respect to the static response. This is because the distance between pole and zero in the open-loop transfer function increases which subsequently leads to a higher control performance even if the feedback gain is constant. In addition, the robustness of RFF and α-controller are generally degraded for any changes in the stiffness of the primary system since the resonance of the control systems has been perfectly tuned for the initial stiffness k_0. It has been already shown in Figures 3 and 12 that any changes in the tuning frequency of RFF ω_f can significantly affect the control performance. On the other hand, the robustness of RFF and α-controller depend on the stiffness ratio $\frac{k_a}{k_0}$ such that the degradation rate of the control performance decreases with increasing in the stiffness ratio $\frac{k_a}{k_0}$. It should be noted that despite the loss of efficiency under the variation of the stiffness (i.e., $\frac{k}{k_0} = [0.6, 1.5]$), the performance of RFF is still superior to that of IFF, which is an appealing feature of RFF. It can be also observed that RFF can tolerate a higher level of uncertainty than α-controller when $k < k_0$.

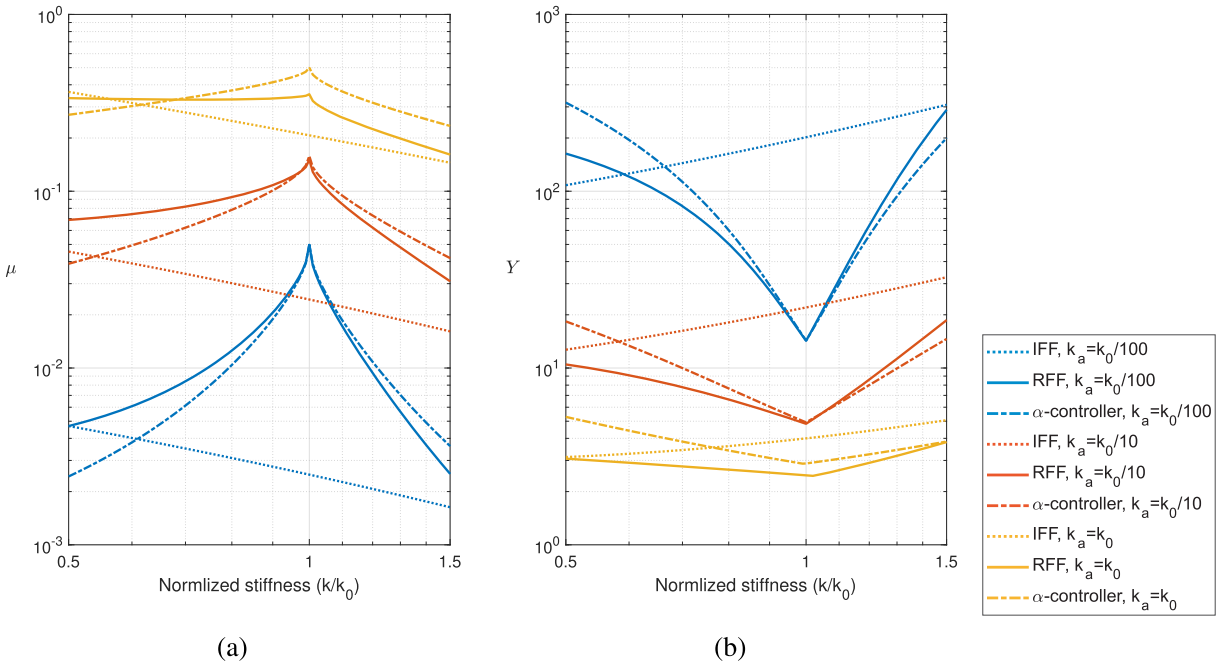

(a) (b)

FIGURE 16 Under the variation of the stiffness k of the primary system while the parameters of the controller are kept constant at their optimal values for the specified stiffness ratios, that is, $k_a/k_0 : 0.01, 0.1, 1$, (a) closed-loop damping coefficient μ of the performance index and (b) normalized maximum amplitude Y of the performance index with respect to the static response

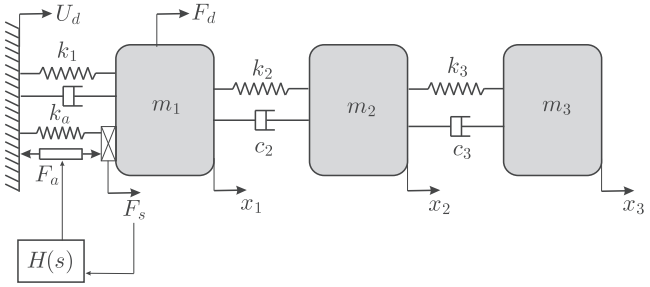

FIGURE 17 Multi-degree-of-freedom (MDOF) system combined with a force actuator and a force sensor for vibration damping

5 | MULTIPLE DEGREE OF FREEDOM SYSTEM

In this section, the performance of the designed RFF is evaluated on a lightly damped system with multiple resonances representing a flexible structure. In particular, a three degree of freedom (DOF) system, as shown in Figure 17, is considered as the numerical example. The following numerical values have been used: $m_1 = m_2 = m_3$=1kg, k_1=100kN/m, $k_a = 0.1K_1$, and $k_2 = k_3$=400kN/m. Note that Dashpot constants c_1, c_2, and c_3 are tuned in order to provide a modal damping ratio of 0.2%. All the mathematics are given in Appendix A1.

For the system under consideration, the frequencies of the poles and the zeros are listed in Table 3. Considering these, an optimal RFF controller is designed for each mode individually according to the method of maximum damping explained in Section 2.5. According to Equation (19), the closed loop damping achieved by an optimal RFF for each mode is also shown in Table 3. The closed-loop damping is compared to that of a system damped by an optimal IFF according to Table 1. It can be seen that higher damping is obtained by RFF especially at higher resonance frequency as the controlability is lower due to close frequencies of pole and zero.

The root-locus for an optimal RFF targeting each mode is shown in Figure 18. One sees that the closed-loop poles are not identical. This is because of the presence of other modes affecting the shape of the loops and the damping of the primary system. For the first and second modes, they are fairly close to each other at the vicinity of the closed loop damping ratio presented in Table 3. In fact, the closed loop poles for the first and second modes are 10% off with respect to a pair of identical closed-loop poles. Targeting the first mode as an example, Figure 19 compares the impulse responses of the optimal RFF to the ideal RFF which provides exactly the same closed-loop poles. It is clear that the differences in terms of the settling time and the amplifications can be negligible. As expected, the closed-loop poles are not placed at the vicinity of 3.9% damping ratio for the third mode. This is because the third resonance is not well separated from the other resonances. Although the poles are not identical providing the desired damping ratio, they are still much higher than the damping ratio obtained by IFF.

It is very interesting to note that the RFF can be used for vibration isolation of the system under a base excitation. Moreover, the method of maximum damping is independent from excitation sources. This means that no matter

TABLE 3 Frequency of pole and zero

Frequencies	Mode 1 [rad/s]	Mode 2 [rad/s]	Mode 3 [rad/s]
Pole	177.4	677.3	1105.9
Zero	170.3	672.4	1102.5
ξ_{IFF}^{opt}	0.02	0.003	0.0015
ξ_{RFF}^{opt}	0.14	0.06	0.039

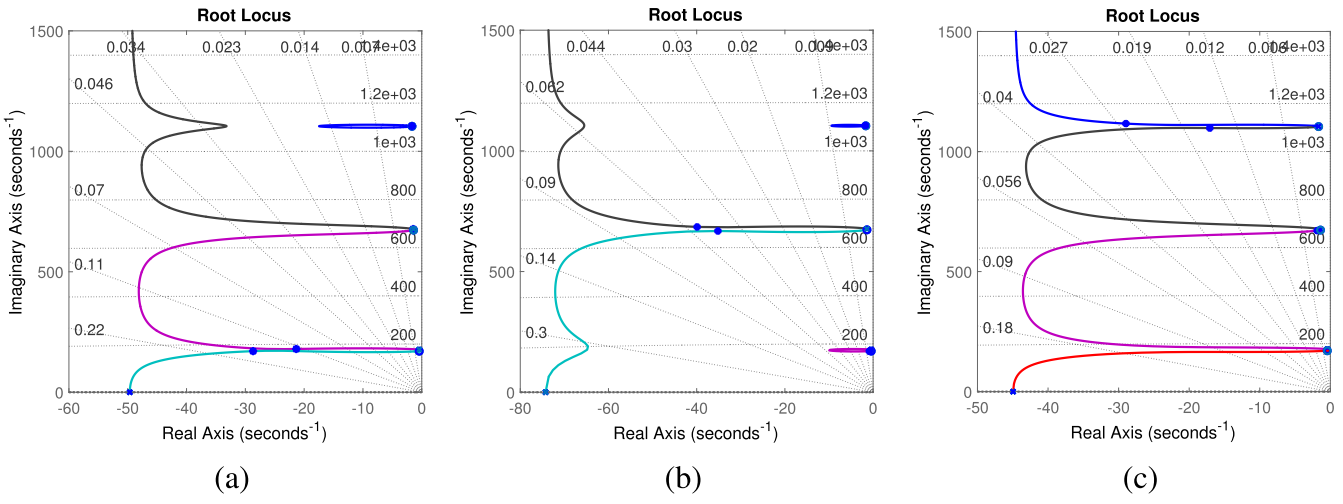

FIGURE 18 Root-locus plot for the resonant-force-feedback (RFF) targeting (a) the first, (b) the second, and (c) the third modes

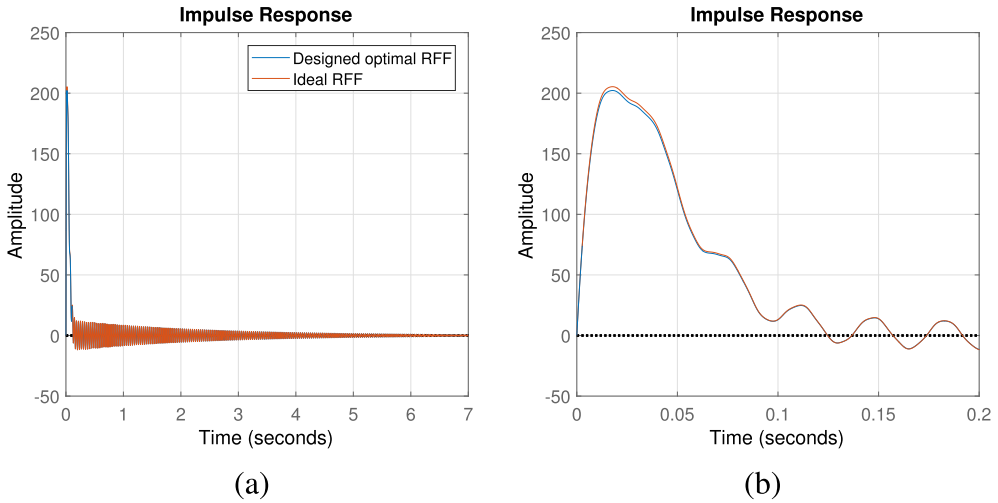

FIGURE 19 Impulse response of the multi-degree-of-freedom (MDOF) system when the optimal resonant-force-feedback (RFF) designed to target the first mode and when an ideal RFF is used

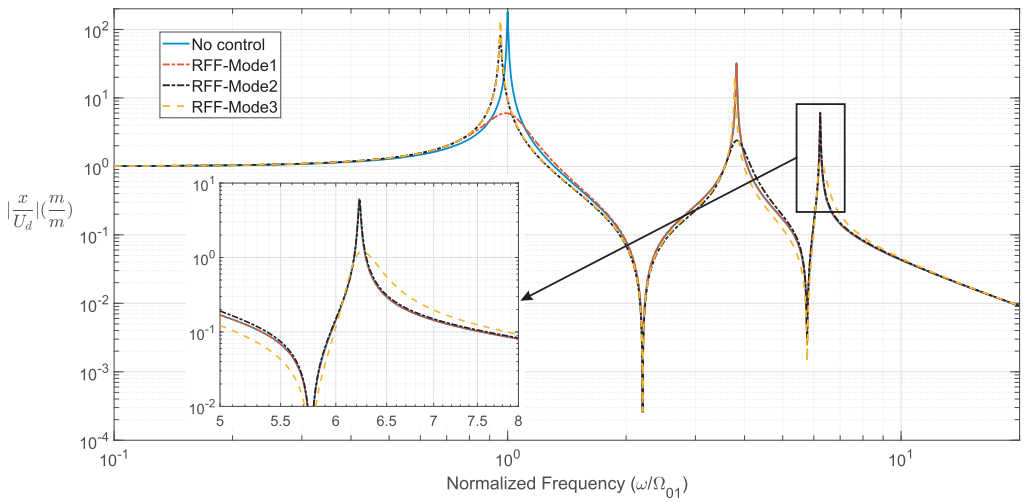

FIGURE 20 Transmisibility of system with and without resonant-force-feedback (RFF)

whether the system is excited by the an external force or the base motion, the RFF can add the designed damping to the system. Figure 20 shows the transmissibility of the system from the base excitation U_d to the displacement of the first mass x_1. The transmissibility compares the response of the system without the control system and with the RFF targeting each mode individually. It can be seen that RFF can effectively damp the modes.

The following section evaluates the performance of the designed RFF in Section 2.6 according to H_∞ optimization on the MDOF system. For this purpose, three optimal RFFs targeting each mode individually are designed according to Equations (22)–(25). The performance index is defined by a transfer function from the disturbance force F_d of the first mass to the displacement at the same location x_1. The FRFs of the performance index are shown in Figure 21 for the system with and without the control system. Note that the frequency is normalized with respect to the frequency of the first resonance. First, one sees that higher vibration reduction at the resonance frequency is achieved by RFF compared to that of IFF. In addition, two equal peaks at the vicinity of the primary resonance frequency can be detected when RFF is applied. The equal peak may be distorted at higher resonance frequency as the modal density increases by frequency in this example.

From Figure 21, it can be seen that the RFF does not have any effect on the resonances above its tuning frequency. This is because the RFF as a low-pass filter suppresses all the high frequency contents. Due to this property, the RFF

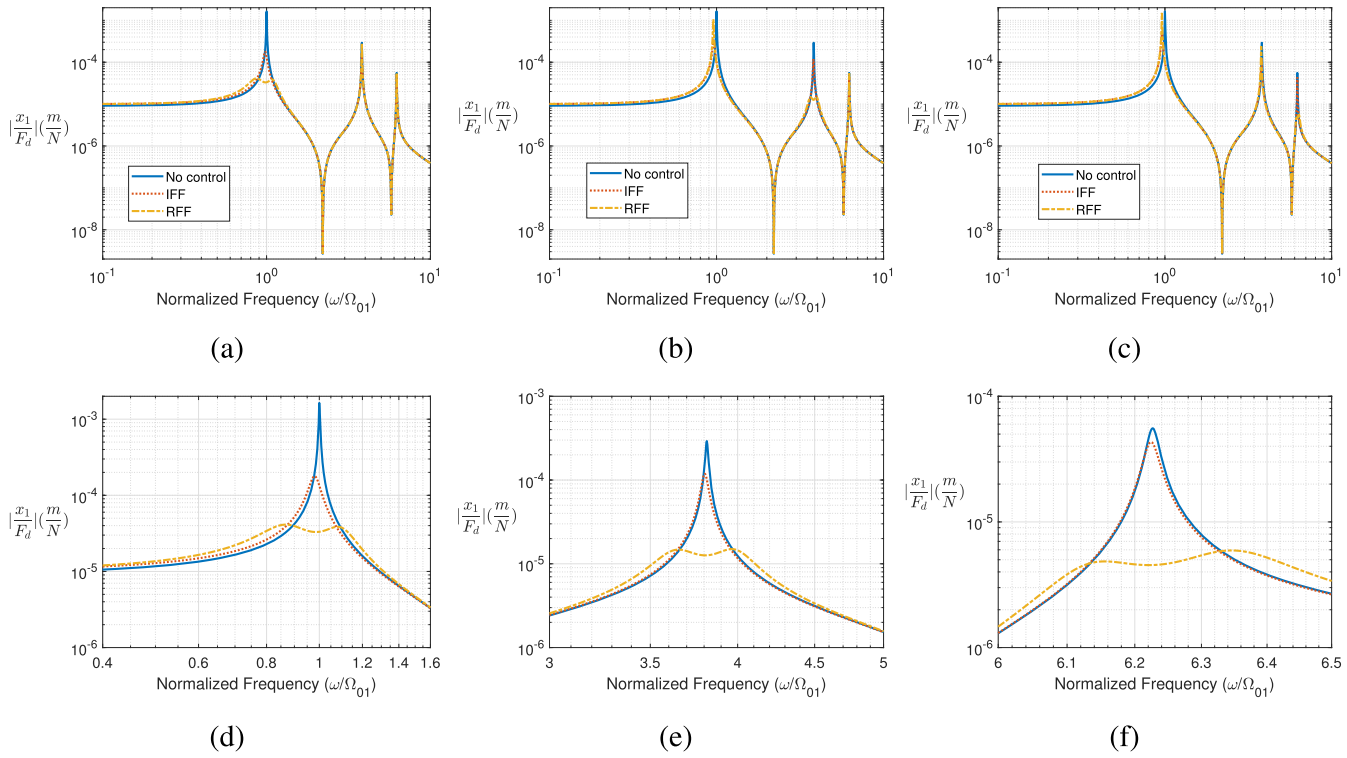

FIGURE 21 Frequency-response-function (FRF) of the performance index when RFF targets (a) the first mode, (b) the second mode, and (c) the third mode. Zoom around (d) the first mode, (e) the second mode, and (f) the third mode

avoids high frequency amplifications (known as spillover) and the saturation of the actuator. However, low frequency contents amplified with respect to the feedback gain are fed back to the actuator. This leads to a decrease in both the static stiffness and the dynamic stiffness of the modes with the frequencies lower than the tuning frequency of the RFF. These resonances are therefore shifted to a lower value.

The optimal RFF tuned according to H_∞ approach is based on the performance index from an external excitation force to a displacement response of the same location. This means that the optimal RFF is no longer be able to provide equal peaks at a resonance of a the system excited from the base.

6 | CONCLUSION

A new resonant control system based on the force feedback configuration, named RFF, has been proposed and optimally designed to overcome performance limitations of the classical IFF when a resonance of a structure is targeted. It has been shown that RFF can be seen as an active realization of an inerter-spring-damping (ISD) system which can also be used for vibration damping, vibration isolation and suspension systems in different applications. Then, its equivalent mass, damping and stiffness have been derived. The controller possess three unknown parameters including the damping coefficient, tuning frequency and feedback gain. These parameters have been optimized according to two different tuning laws i.e. the method of maximum damping and H_∞ optimization. The closed-form expressions of these parameters have been obtained for a single-degree-of-freedom (SDOF) system. It has been shown that second order filter as the control law in the feedback loop from the force sensor to the force actuator leads to the design of an absorber with an excellent performance. Therefore, the control authority of a target mode can be significantly increased using RFF in comparison to IFF. In addition, since α-controller is another control law to offer a better control performance than the classical IFF, the performance of RFF has been evaluated in comparison to that of α-controller in terms of the vibration mitigation and the control effort. Although both techniques provide almost the same control authority, RFF requires less actuator force than α-controller. Therefore, RFF can be considered as a low energy consumption technique to enhance the vibration mitigation of flexible structures using force feedback. It has been also demonstrated in the

robustness analysis that RFF brings a superior performance to that of IFF up to almost 50% changes in the stiffness of the primary system while IFF can tolerate a higher level of uncertainty.

It is interesting to note that RFF can be used for vibration isolation under a base excitation.

ACKNOWLEDGEMENT

The authors are grateful to the financial support of MAVERIC (Wal'innov project 1610122).

AUTHOR CONTRIBUTIONS

Ahmad Paknejad: Conceptualization; methodology; software; visualization; writing – original draft. **Guoying Zhao:** Review & editing. **Simon Chesné**: Investigation; review & editing. **Arnaud Deraemaeker:** Investigation, review & editing. **Christophe Collette:** Review & editing; funding acquisition; supervision.

ORCID

Ahmad Paknejad https://orcid.org/0000-0003-2920-144X

REFERENCES

1. Moheimani SOR, Halim D, Fleming AJ. *Spatial control of vibration: theory and experiments*, Vol. 10: World scientific; 2003.
2. Moheimani SOR, Fleming AJ. *Piezoelectric transducers for vibration control and damping*: Springer Science & Business Media; 2006.
3. Jones DIG. *Handbook of viscoelastic vibration damping*: John Wiley & Sons; 2001.
4. Hagood NW, von Flotow A. Damping of structural vibrations with piezoelectric materials and passive electrical networks. *J Sound Vib*. 1991;146(2):243-268.
5. Ao WK, Reynolds P. Evaluation of optimal analysis, design, and testing of electromagnetic shunt damper for vibration control of a civil structure. *Struct Control Health Monit*. 2020;27(3):e2495.
6. Li D, Tang H, Xue S. Robust design of tuned mass damper with hybrid uncertainty. *Struct Control Health Monit*. 2021;28(10):e2803.
7. Zhang C, Wang H. Swing vibration control of suspended structures using the active rotary inertia driver system: theoretical modeling and experimental verification. *Struct Control Health Monit*. 2020;27(6):e2543.
8. Forward RL. Electromechanical transducer-coupled mechanical structure with negative capacitance compensation circuit. Google Patents, US Patent 4,158,787. 1979.
9. Preumont A. *Vibration control of active structures*, Vol. 2: Springer; 1997.
10. Ahmadi MW. Preventing stroke saturation of inertial actuators used for active vibration control of floor structures. *Struct Control Health Monit*. 2020;27(7):e2546.
11. Paknejad A, Zhao G, Osée M, Deraemaeker A, Robert F, Collette C. A novel design of positive position feedback controller based on maximum damping and h 2 optimization. *J Vib Control*. 2020;26:1077546319892755.
12. Preumont A, Dufour J-P, Malekian C. Active damping by a local force feedback with piezoelectric actuators. *J Guid, Control, Dyn*. 1992;15(2):390-395.
13. Zhao G, Paknejad A, Deraemaeker A, Collette C. h_∞ optimization of an integral force feedback controller. *J Vib Control*. 2019;25(17):2330-2339.
14. Teo YR, Fleming AJ. Optimal integral force feedback for active vibration control. *J Sound Vib*. 2015;356:20-33.
15. Chesné S, Milhomem A, Collette C. Enhanced damping of flexible structures using force feedback. *J Guid, Control, Dyn*. 2016;39(7):1654-1658.
16. Zhao G, Raze G, Paknejad A, Deraemaeker A, Kerschen G, Collette C. Active tuned inerter-damper for smart structures and its h_∞ optimisation. *Mech Systems Sig Process*. 2019;129:470-478.
17. Monnier P, Collet M, Piranda J. Definition of mechanical design parameters to optimize efficiency of integral force feedback. *Struct Control Health Monit*. 2005;12(1):65-89.
18. Smith MC. Synthesis of mechanical networks: the inerter. *IEEE Trans Autom Control*. 2002;47(10):1648-1662.
19. Sun W, Thompson D, Zhou J. A mechanism for overcoming the effects of the internal resonances of coil springs on vibration transmissibility. *J Sound Vib*. 2020;471:115145.
20. Chen MiZQ, Papageorgiou C, Scheibe F, Wang F-C, Smith MC. The missing mechanical circuit element. *IEEE Circ Syst Mag*. 2009;9(1):10-26.
21. Papageorgiou C, Houghton NE, Smith MC. Experimental testing and analysis of inerter devices. *J Dyn Syst, Meas, Control*. 2009;131(1):011001-1-011001-11.
22. Liu X, Jiang JZ, Titurus B, Harrison A. Model identification methodology for fluid-based inerters. *Mech Syst Sig Process*. 2018;106:479-494.
23. Swift SJ, Smith MC, Glover AR, Papageorgiou C, Gartner B, Houghton NE. Design and modelling of a fluid inerter. *Int J Control*. 2013;86(11):2035-2051.
24. De Marneffe B, Avraam M, Deraemaeker A, Horodinca M, Preumont A. Vibration isolation of precision payloads: a six-axis electromagnetic relaxation isolator. *J Guid, Control, Dyn*. 2009;32(2):395-401.

25. Fleming AJ, Behrens S, Moheimani SOR. Reducing the inductance requirements of piezoelectric shunt damping systems. *Smart Mater Struct*. 2003;12(1):57.
26. Zhou S, Jean-Mistral C, Chesné S. Electromagnetic shunt damping with negative impedances: optimization and analysis. *J Sound Vib*. 2019;445:188-203.
27. Lazar IF, Neild SA, Wagg DJ. Using an inerter-based device for structural vibration suppression. *Earthq Eng Struct Dyn*. 2014;43(8): 1129-1147.
28. Zhang R, Zhao Z, Pan C, Ikago K, Xue S. Damping enhancement principle of inerter system. *Struct Control Health Monit*. 2020;27(5): e2523.
29. Wang Y, Meng H, Zhang B, Wang R. Analytical research on the dynamic performance of semi-active inerter-based vibration isolator with acceleration–velocity-based control strategy. *Struct Control Health Monit*. 2019;26(4):e2336.
30. Høgsberg J, Brodersen ML, Krenk S. Resonant passive–active vibration absorber with integrated force feedback control. *Smart Mater Struct*. 2016;25(4):047001.
31. Bani-Hani KA. Vibration control of wind-induced response of tall buildings with an active tuned mass damper using neural networks. *Struct Control Health Monit*. 2007;14(1):83-108.
32. Alujevic N, Catipovic I, Wolf H, Vladimir N. Synthesis of the inerter by direct acceleration feedback. In: Proceedings of 23rd international congress on acoustic, Physical aspects for active control of noise and vibration; 2019; Aachen, Germany.
33. Zhao G, Paknejad A, Raze G, Deraemaeker A, Kerschen G, Collette C. Nonlinear positive position feedback control for mitigation of nonlinear vibrations. *Mech Syst Sig Process*. 2019;132:457-470.
34. Fleming AJ, Behrens S, Moheimani SOR. Synthetic impedance for implementation of piezoelectric shunt-damping circuits. *Electron Lett*. 2000;36(18):1525-1526.
35. Paknejad A, Zhao G, Chesné S, Deraemaeker A, Collette C. Hybrid electromagnetic shunt damper for vibration control. *J Vib Acoust*. 2020;143(2):021010-1-021010-11.
36. Yang J, Jiang JZ, Zhu X, Chen H. Performance of a dual-stage inerter-based vibration isolator. *Procedia Eng*. 2017;199:1822-1827.
37. Ramakrishnan K, Yang L, Ballo FM, Gobbi M, Mastinu G. Multi-objective optimization of road vehicle passive suspensions with inerter. In: Asme 2016 international design engineering technical conferences and computers and information in engineering conference American Society of Mechanical Engineers Digital Collection; 2016.
38. Jiang JZ, Matamoros-Sanchez AZ, Goodall RM, Smith MC. Passive suspensions incorporating inerters for railway vehicles. *Veh Syst Dyn*. 2012;50(sup1):263-276.
39. Li Y, Jiang JZ, Neild S. Inerter-based configurations for main-landing-gear shimmy suppression. *J Aircraft*. 2017;54(2):684-693.
40. Den Hartog JP. *Mechanical vibrations*: Courier Corporation; 1985.
41. Crandall SH, Mark WD. *Random vibration in mechanical systems*: Academic Press; 1963.

How to cite this article: Paknejad A, Zhao G, Chesné S, Deraemaeker A, Collette C. Design and optimization of a novel resonant control law using force feedback for vibration mitigation. *Struct Control Health Monit*. 2022; 29(6):e2939. doi:10.1002/stc.2939

APPENDIX A: MATHEMATICS OF MDOF

A state-space system is modeled for the MDOF system with the inputs including the disturbance force F_d, the base excitation U_d, and the actuator force F_a and with the outputs including the displacement of the first mass x_1 and the force sensor F_s. The matrices are given below:

$$A=\begin{bmatrix} 0 & 1 & 0 & 0 & 0 & 0 & 0 \\ -\frac{k_1+k_2+k_a}{m_1} & -\frac{c_1+c_2}{m_1} & \frac{2}{m_1} & \frac{c_2}{m_1} & 0 & 0 & 0 \\ 0 & 0 & 0 & 1 & 0 & 0 & 0 \\ \frac{k_2}{m_2} & \frac{c_2}{m_2} & -\frac{k_2+k_3}{m_2} & -\frac{c_2+c_3}{m_2} & \frac{k_3}{m_2} & \frac{c_3}{m_2} & 0 \\ 0 & 0 & 0 & 0 & 0 & 1 & 0 \\ 0 & 0 & \frac{k_3}{m_3} & \frac{c_3}{m_3} & -\frac{k_3}{m_3} & -\frac{c_3}{m_3} & 0 \\ -k_a & 0 & 0 & 0 & 0 & 0 & 0 \end{bmatrix} \tag{A1}$$

$$B=\begin{bmatrix} 0 & 0 & 0 \\ \frac{1}{m_1} & \frac{1}{m_1} & \frac{k_1+k_a}{m_1} \\ 0 & 0 & 0 \\ 0 & 0 & 0 \\ 0 & 0 & 0 \\ 0 & 0 & 0 \\ 0 & 1 & k_a \end{bmatrix} \tag{A2}$$

$$C=\begin{bmatrix} 1 & 0 & 0 & 0 & 0 & 0 & 0 \\ -k_a & 0 & 0 & 0 & 0 & 0 & 0 \end{bmatrix} \tag{A3}$$

$$D=\begin{bmatrix} 0 & 0 & 0 \\ 0 & 1 & k_a \\ 0 & 0 & 0 \\ 0 & 0 & 0 \end{bmatrix} \tag{A4}$$